IOP Publishing Journal of Physics D: Applied Physics

J. Phys. D: Appl. Phys. **51** (2018) 475501 (9pp) https://doi.org/10.1088/1361-6463/aae336

Synthesis of NiO–Co_3O_4 nanosheet and its temperature-dependent supercapacitive behavior

Nilesh G Saykar[1], Ritu Kumari Pilania[1], I Banerjee[2] and S K Mahapatra[1,3]

[1] Department of Physical Sciences, Central University of Punjab, Bathinda 151001, India
[2] School of Nano Sciences, Central University of Gujarat, Gandhinagar 382030, India

E-mail: skmahapatra741973@gmail.com

Received 22 July 2018, revised 10 September 2018
Accepted for publication 21 September 2018
Published 9 October 2018

Abstract

A nanosheet of nickel and cobalt double hydroxides (NC RT) has been synthesized by the facile hydrothermal method. It has been treated at temperatures of 300 °C, 400 °C and 500 °C, namely NC 300, NC 400 and NC 500, respectively, to obtain a nanosheet of NiO–Co_3O_4. Samples have been investigated using XRD, Raman spectroscopy, FESEM and TEM. It can be observed that nickel hydroxide is converted to NiO at 300 °C, whereas cobalt hydroxide is converted to Co_3O_4 at 400 °C. The double hydroxide nanosheet leads to porous oxide nanosheet at an elevated temperature. The formation of porous structure could be attributed to the rapid release of water molecules during thermal treatment. Four symmetric supercapacitors are prepared with NC RT, NC 300, NC 400 and NC 500 as electrode materials, keeping 3 M KOH as an electrolyte and Whatman filter paper as a separator for all the symmetric supercapacitors. It can be seen that the specific capacitances of the NC RT, NC 300, NC 400 and NC 500 symmetric supercapacitors are decreased with increasing temperature in the range of 25 °C–80 °C and scan rate in the range of 10–500 mV s^{-1}. It can be seen that the NC 300 has excellent supercapacitive behavior. The specific capacitance of NC RT decreased from 20 to 6 F g^{-1}, NC 300 decreased from 324 to 57 F g^{-1}, NC 400 decreased from 132 to 61 F g^{-1} and NC 500 decreased from 81 to 48 F g^{-1} with the variation of scan rate from 10–500 mV s^{-1}. The decrement in the specific capacitance may be attributed to the increased bulk and charge transfer resistance at elevated temperature.

Keywords: NiO–Co_3O_4, symmetric supercapacitor, hydrothermal

(Some figures may appear in colour only in the online journal)

Introduction

Owing to the increasing demand for energy and growing environmental issues due to the tremendous use of fossil fuels, the development of an environmentally-friendly high-efficiency storage system is a requisite. Electrochemical supercapacitors, Li-ion, Na-ion and Ni–H batteries have the potential to solve the aforementioned environmental issues [1–3]. Among all these candidates, supercapacitors have received a considerable amount of attention due to their higher power density, faster charge–discharge property, longer cycle life and simple ease of fabrication compared to traditional batteries [1, 4–6].

In the field of supercapacitors, a large number of materials including carbon-based materials, transition metal oxides [7–9] and hybrid composites [10, 11], are utilized to achieve higher efficiency. The materials such as RuO_2 show higher efficiency, but higher efficiency should not comprise higher cost and environmental hazard. From this point of view, the entire scientific community is seeking inexpensive, environmentally-friendly transition metal oxides with good capacitive characteristics. Materials possessing multiple oxidation

[3] Author to whom any correspondence should be addressed.

states/structures that enable rich redox reactions, such as Co_3O_4, NiO, MnO_2, hydroxide-based composites and Co_3O_4/NiO core/shell nanowire arrays are capable of being used in a commercial application. In addition, NiO and Co_3O_4 are extensively used in supercapacitor applications due to their unique properties of physical and chemical stability. One attempt is made to develop layered double hydroxide (LDH) of nickel and cobalt because its crystal structure is made up of positively charged host layers. The interlayer charge, compensating anions and solvation molecules present between the host layer help to promote the deep ion diffusion among electrodes, with a consequent increment in capacitance [12].

The literature reveals that composite of NiO and Co_3O_4 is a better electrode material for the supercapacitor due its electrical, physical and chemical stability. Wang *et al* synthesized microspheres of NiO and Co_3O_4 composite having a surface area of 164.9 $m^2\ g^{-1}$ and an achieved specific capacitance of 801 F g^{-1} at a current density of 1 A g^{-1} [5]. Liu *et al* synthesized flower-like NiO–Co_3O_4 composite having a specific capacitance of 1988.6 F g^{-1} at 1 A g^{-1} with a surface area of 164.9 $m^2\ g^{-1}$ and 94% capacitance retention up to 1500 cycles at 10 A g^{-1} [13]. 1D wire-like NiO–Co_3O_4 composite, synthesized by Liu T *et al*, has a specific capacitance of 184 F g^{-1} at a current density of 1 A g^{-1} [14]. Flower-like mesoporous NiO–Co_3O_4 provides a specific capacitance of 1190 F g^{-1} with a 56.9 $m^2\ g^{-1}$ surface area, at a current density of 4 A g^{-1} and 99% capacitance retention up to 5000 cycles [15]. The NiO–Co_3O_4 core/shell composites provide specific capacitance of 510 F g^{-1} at a current density of 5 mA cm^{-2} and possess 92% capacitance retention even after 1000 cycles [16]. NiO microcubes anchored on Co_3O_4 nanowires prepared by Zhou *et al* exhibit a specific capacitance of 2691 mF cm^{-2} at 2 mA cm^{-2} and 84.62% capacitance retention up to 2000 cycles. An asymmetric supercapacitor prepared using NiO nanowires exhibits an energy density of 26.03 Wh kg^{-1} at a power density of 374.83 W kg^{-1} [17]. NiO@Co_3O_4 nanofibers having a 136.9 $m^2\ g^{-1}$ specific surface area provide a specific capacitance of 788 F g^{-1} at a current density of 5 mA cm^{-2} with 93% retention after 1000 cycles [18]. However, study on the temperature-dependent capacitive behavior of NiO–Co_3O_4 nanocomposite is rare.

In this paper, we synthesized a nanosheet of nickel and cobalt double hydroxides (NC RT) using the hydrothermal method. This nanosheet of nickel and cobalt hydroxides is treated at temperatures of 300 °C, 400 °C and 500 °C, namely NC 300, NC 400 and NC 500, respectively, to obtain a nanosheet of NiO–Co_3O_4. Samples have been investigated using XRD, Raman spectroscopy, FESEM and TEM. Four symmetric supercapacitors are prepared with NC RT, NC 300, NC 400 and NC 500 as electrode materials, keeping 3 M KOH as an electrolyte and Whatman filter paper as a separator for all the symmetric supercapacitors. It can be observed that NC 300 shows better capacitive behavior than any of the other symmetric supercapacitors. It can be seen that the specific capacitances of NC RT, NC 300, NC 400 and NC 500 are decreased with the scan rate in the range of 10–500 mV s^{-1} and an increase of temperature of the symmetric supercapacitor in the range of 25 °C–80 °C.

Experimental details

Synthesis of Ni-rich NiO–Co_3O_4

320 mg of $Ni(NO_3)_2{\cdot}6H_2O$ and 132 mg of urea are dissolved into 40 ml of a mixed solvent of deionized water and methanol in the ratio 3:2. The mixture is subjected to an intense ultrasonic treatment for a few minutes and then 160 mg of $Co(NO_3)_2{\cdot}6H_2O$ is dissolved into the above solution under constant magnetic stirring to form a homogeneous pink solution. After that, the obtained pink solution is transferred to 50 ml Teflon-lined stainless-steel autoclaves and maintained at 140 °C for 12 h. The solution is cooled to room temperature; the solid product is collected by centrifugation and washed with distilled water and ethanol several times, and then dried in a vacuum oven at 60 °C for 6 h. This final product is known as NC RT. The NC RT is calcinated at three different temperatures of 300 °C, 400 °C and 500 °C with a ramping rate of 5 °C min^{-1} in air for 3 h. In this way, three samples, namely NC 300, NC 400 and NC 500 are obtained through the three calcination temperatures of 300 °C, 400 °C and 500 °C, respectively.

Fabrication of the symmetric supercapacitor

The electrode of the symmetric supercapacitor is fabricated by mixing NC RT, carbon black and polyvinylidene fluoride binder in a weight ratio of 70:20:10 on a piece of Ni foam and dried under vacuum at 80 °C for 12 h to remove N-methyl-2-pyrrolidone (NMP). In this way, four types of electrodes are prepared with NC RT, NC 300, NC 400 and NC 500 samples. Whatman filter paper, dipped in 3 M KOH solution and dried at room temperature, is used as a separator. A symmetric supercapacitor is prepared by sandwiching two electrodes with a separator by using a hydraulic press machine. Through this method, we prepared four symmetric supercapacitors with NC RT, NC 300, NC 400 and NC 500 as electrode materials, keeping 3 M KOH as an electrolyte and Whatman filter paper as a separator for all the supercapacitors.

Measurement

Morphology of the samples is observed by high-resolution FESEM (Carl Zeiss Merlin Compact). Particle size and crystal structure of the NC samples were obtained using TEM (TECNAI G2). The structural analysis is carried out through XRD spectra (PANanalytical) and Raman spectra obtained using a Renishaw Raman spectrometer at a laser wavelength of 532 nm. Brunauer–Emmett–Teller (BET) nitrogen adsorption–desorption is used to calculate the surface area of the sample. Pore size distribution in the material is estimated using Barrett–Joyner–Halenda (BJH) methods (Quantachrome Autosorb iQ Station).

Electrochemical measurement

Electrochemical measurements are performed using a CHI 760E electrochemical workstation (ChenHua Corp., Shanghai,

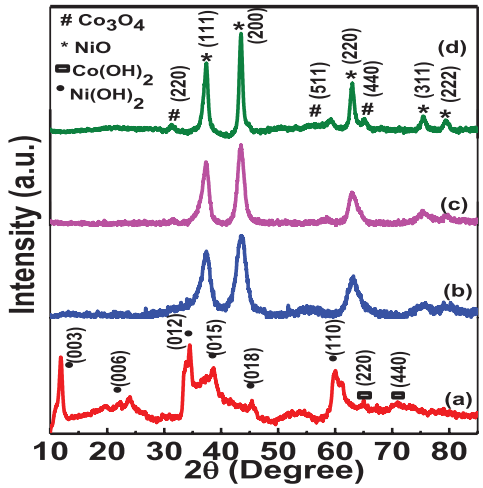

Figure 1. XRD spectra of (a) NC RT, (b) NC 300, (c) NC 400 and (d) NC 500.

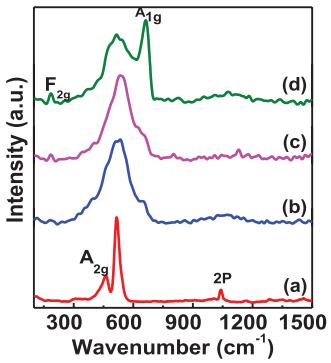

Figure 2. Raman spectra of (a) NC RT, (b) NC 300, (c) NC 400 and (d) NC 500 in the range of 100–1500 cm^{-1}.

China). Cyclic voltammetry (CV) and charging–discharging measurements are recorded by the two-electrode system. CV is performed within a potential range of −0.5–0.5 V at scan rates from 10–500 mV s^{-1} at room temperature. In a similar way, CV measurements of the symmetric supercapacitors at different temperatures of 40 °C, 60 °C, 80 °C and cooled to 25 °C are obtained in the potential window −0.5–0.5 V (scan rate 50 mV s^{-1}). Galvanostatic charge–discharge is tested at different current densities 2, 3, 4 and 6 A g^{-1} of all the samples with a potential embedded between −0.5–0.5 V.

Result and discussion

Figure 1 shows XRD spectra of NC obtained from (a) NC RT, (b) NC 300, (c) NC 400 and (d) NC 500. Figure 1(a) shows the diffraction peaks at 11.8°, 22.33°, 34.49°, 38.68°, 45.38° and 60.08° corresponding to the (0 0 3), (0 0 6), (0 1 2), (0 1 5), (0 1 8) and (1 1 0) planes of α-Nickel hydroxide hydrate (JCPDS card no-380715) and the peaks at 64.94°, 67.39° and 70.94° corresponding to the (2 2 0), (5 1 1) and (4 4 0) planes of α-cobalt hydroxide [19]. This confirms the formation of LDH. Figure 1(b) shows new peaks at 37.3°, 43.3°, 62.9°, 75.37° and 79.34° corresponding to the (1 1 1), (2 0 0), (2 2 0), (3 1 1) and (2 2 2) planes of the face-centered cubic phase of NiO (JCPDS Card no. 47-1049). The peaks positioned at 75.37° and 79.34° are not prominent, but are found to be prominent in the samples treated at 400 °C and 500 °C, as shown in figures 1(c) and (d). In addition, new peaks at 31.3°, 59.4° and 65.2° belong to the (2 2 0), (5 1 1) and (4 4 0) planes of the cubic phase of Co_3O_4 (JCPDS Card no. 42-1467) in the samples treated at 400 °C and 500 °C, as shown in figures 1(c) and (d). This confirms the formation of NiO in the 300 °C treated sample and the formation of NiO with Co_3O_4 in the 400 °C and 500 °C treated samples. From the XRD plots, it is clear that there has been complete transformation of the LDH of nickel and cobalt to NiO and Co_3O_4 at the optimum temperature of ~400 °C, which converts to a higher crystalline form at the temperature 500 °C. The average crystalline sizes of the NC 300, NC 400 and NC 500 samples are 0.089, 0.11 and 0.18 nm, respectively, calculated from the Debye–Scherer formula. The crystalline size increased with increasing calcination temperature.

Figure 2 shows Raman spectra in the range 100–1500 cm^{-1} of (a) NC RT, (b) NC 300, (c) NC 400 and (d) NC 500. It can be observed that two Raman bands at 462 and 516 cm^{-1} correspond to the Ni–OH/Co–OH and Ni–O/Co–O stretching modes seen in the Raman spectra. The peak at 1041 cm^{-1} corresponding to OH deformation is shown in figures 2(a)–(c) [20]. The sharp peak at 462 cm^{-1} is observed in the NC RT, whereas it disappeared in the NC 300, NC 400 and NC 500. At the same time, a new peak appeared at 663 cm^{-1} corresponding to the A_{1g} mode of Co_3O_4, which becomes prominent in the NC 500. The shifting of the A_{1g} mode towards the lower frequency may be due to the greater ambience of NiO or substitution of Ni^{2+} at the octahedral site [21]. The peak at 1041 cm^{-1} in figure 2(a) and 1083 cm^{-1} in figure 2(c) corresponds to the 2P mode of the Ni–O [6]. The peak at 184 cm^{-1} observed in figures 2(c) and (d) corresponds to the F_{2g} mode of Co_3O_4. This confirms that the double hydroxide of Ni and Co converted to NiO and hydroxide of Co at 300 °C, NiO and hydroxide of Co converted to NiO and Co_3O_4 at 400 °C, NiO and Co_3O_4 to highly crystalline NiO and Co_3O_4 at 500 °C.

Figure 3 shows FESEM images of (a) NC RT, (b) NC 300, (c) NC 400 and (d) NC 500. Nanosheets are observed in all samples. Dense nanosheets are observed in NC 300 when compared with the NC RT. Chen *et al* also observed similar morphology in the synthesis of LDH nanosheets of Ni–Co composite [12]. Figures 3(c) and (d) show pores in the nanosheets. The pore size is greater in the NC 500 compared to the NC 400. The appearance of the porous structure is due to the rapid release of water molecules during the transformation of both LDH to NiO and Co_3O_4 at elevated temperatures [22].

The micrograph in figure 4 shows a high-magnification TEM image of NC nanosheets. The as-prepared NC composite is formed in ultrathin nanosheets. It can also be seen that the synthesized composite has pores. The crystal structure determination is carried out by estimating the inter-planar distance from the selected-area electron diffraction (SAED) pattern. As the XRD study reveals the NiO–Co_3O_4 composite formation, the SAED pattern (shown in inset) has a similar mixed diffraction pattern from both NiO and Co_3O_4. The SAED pattern of

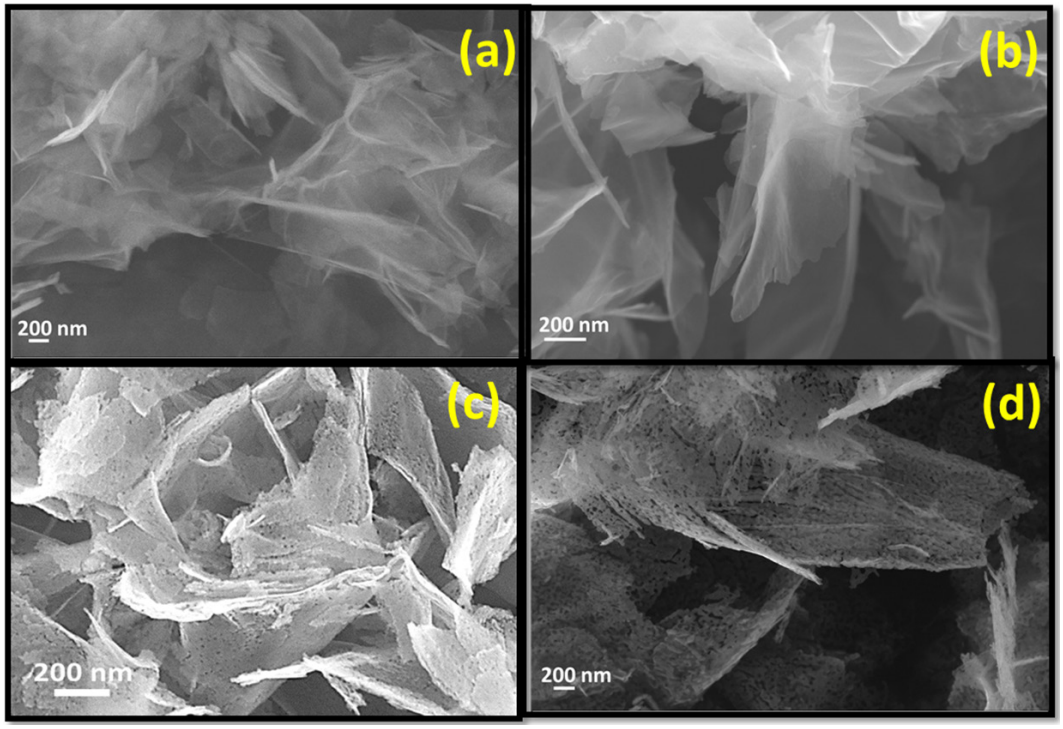

Figure 3. FESEM images of (a) NC RT, (b) NC 300, (c) NC 400 and (d) NC 500.

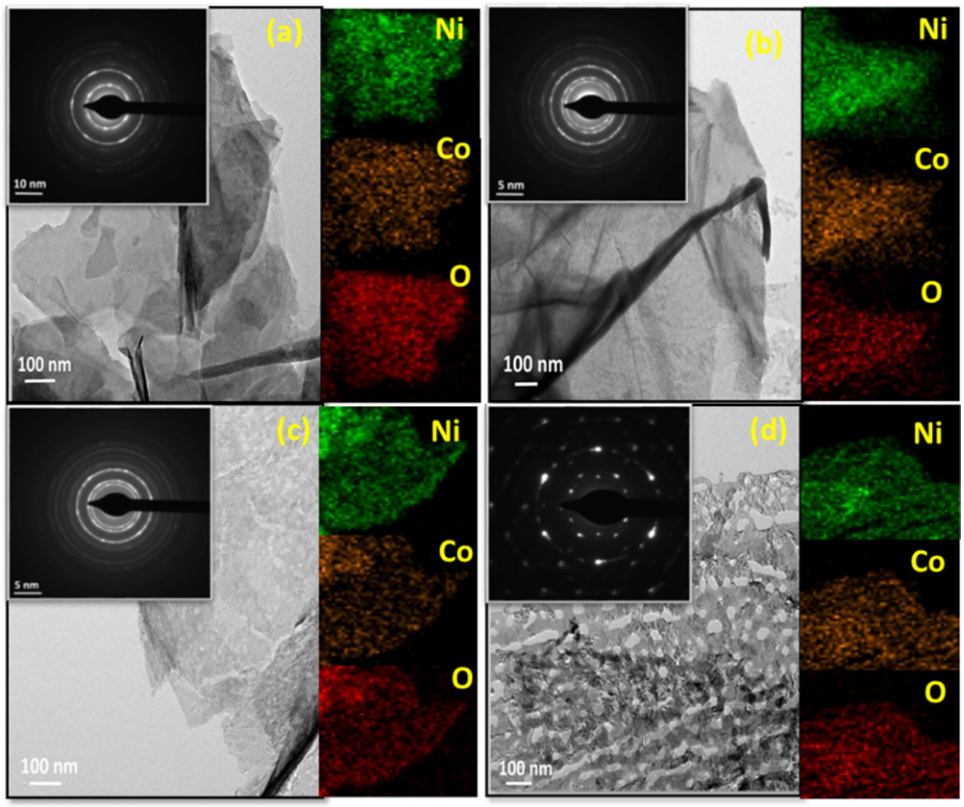

Figure 4. TEM micrographs, elemental mapping (inset) and SAED pattern (inset) of (a) NC RT, (b) NC 300, (c) NC 400 and (d) NC 500.

NC RT, NC 300 and NC 400 shows a broad diffused ring pattern, which confirms the existence of polycrystalline LDH and NiO–Co_3O_4. However, NC 500 exhibits a highly crystalline SAED pattern. The planes (1 1 1), (2 2 0), (3 1 1), (4 2 0) and (2 2 0) with lattice spacing 2.43, 1.46, 1.24, 0.93 and 2.85 Å, respectively, present in NC 500 corresponds to the cubic structure of both NiO and Co_3O_4. The elemental mapping of NC composites is also shown in the inset, which reveals that the nanosheets are formed of both NiO and Co_3O_4 and both are uniformly arranged in the nanosheet.

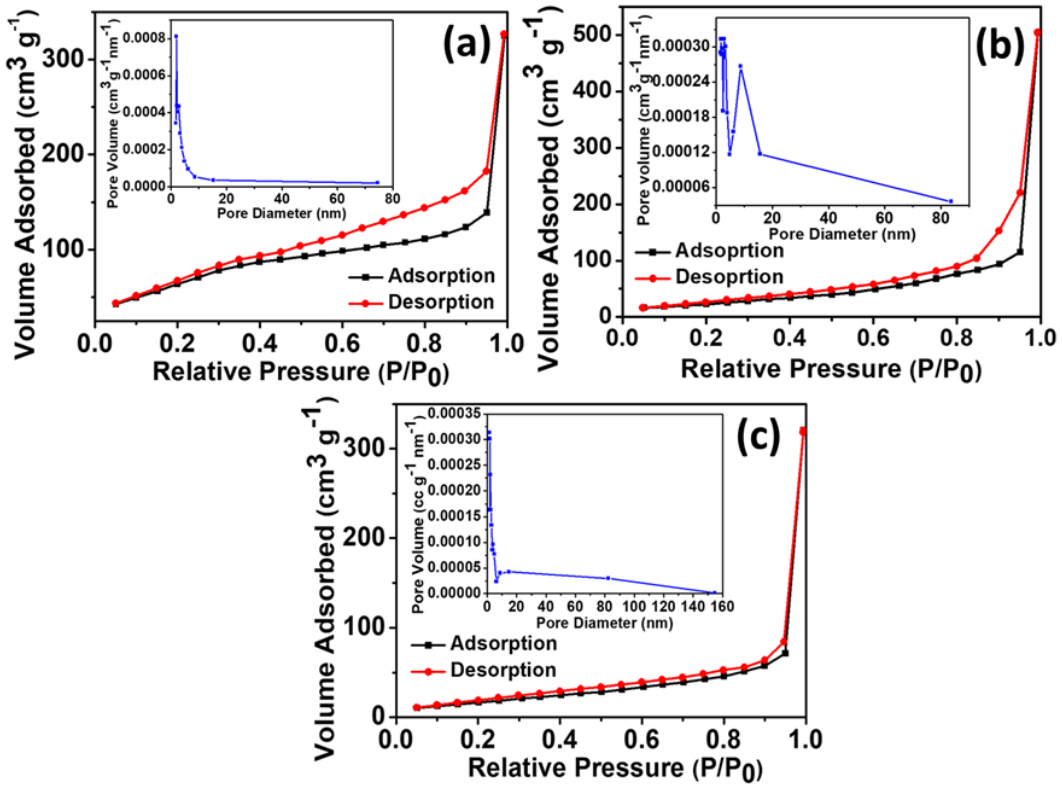

Figure 5. N_2 adsorption/desorption isotherms and pore size distribution curve (inset) of (a) NC 300, (b) NC 400 and (c) NC 500.

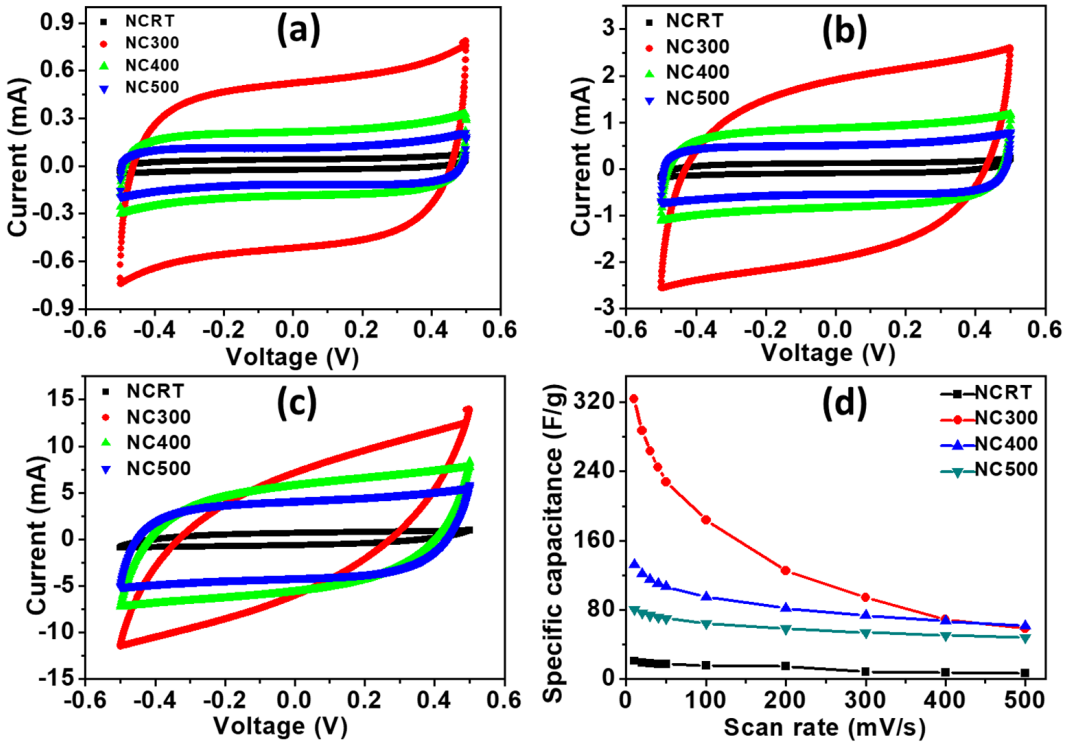

Figure 6. CV plots of NC RT, NC 300, NC 400 and NC 500 at different scan rates of (a) 10 mV s^{-1}, (b) 50 mV s^{-1}, (c) 500 mV s^{-1} and (d) specific capacitance versus scan rates.

The surface area and pore size of NC 300, NC 400 and NC 500 are estimated using the BET and BJH methods. The nitrogen adsorption–desorption isotherms of all the samples are carried out at 77 K and shown in figure 5. The estimated specific surface areas of NC 300, NC 400 and NC 500 are found to be 247.06, 87.15 and 67.69 m^2 g^{-1}, respectively. The hysteresis loop in the isotherm curve of NC 300 exhibits a soft hump between a 0.4 and 1.0 value of P/P_0, as shown in figure 5(a). In a similar way, NC 400 and NC 500 exhibit soft humps between 0.7 and 0.95 and 0.8 and 0.9 of P/P_0, as shown

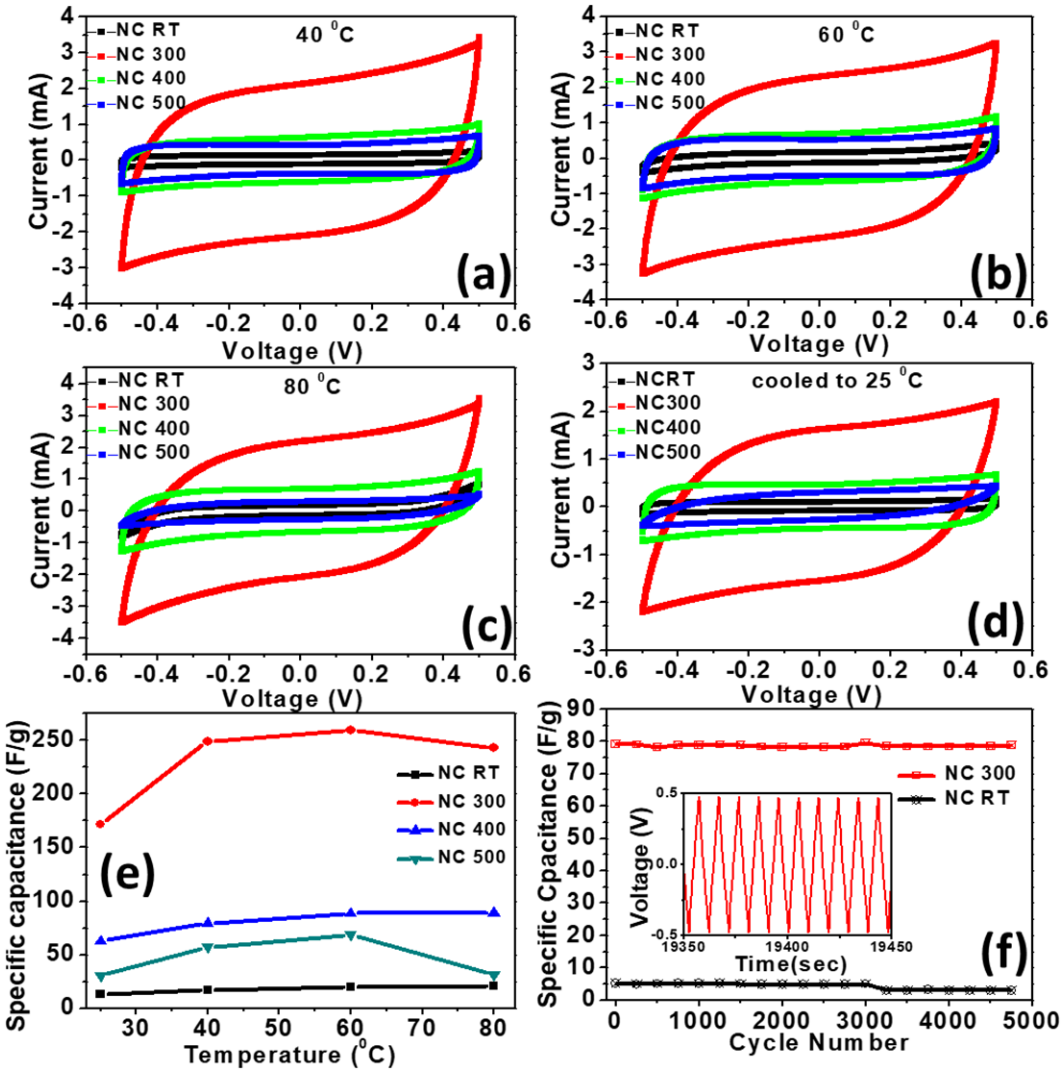

Figure 7. CV plots of NC RT, NC 300, NC 400 and NC 500 at (a) 40 °C, (b) 60 °C, (c) 80 °C and (d) after being cooled at 25 °C. (e) Specific capacitance versus temperature and (f) specific capacitance versus cycle number.

in figures 5(b) and (c), respectively. The inset of figure 5 shows the plot of pore size distribution. The inset in figure 5(a) shows that NC 300 is mesoporous in nature with pore sizes of 1.9 and 2.82 nm, while, NC 400 is also mesoporous in nature with pore sizes of 2.81 and 8.87 nm (inset of figure 5(b)). In a similar way, NC 500 has pore sizes of 2.12, 3.83 and 8.7 nm (inset of figure 5(c)).

CV plots of NC RT, NC 300, NC 400 and NC 500 at different scan rates of (a) 10, (b) 50, (c) 500, and (d) specific capacitance versus scan rates are shown in figure 6. All CV plots are rectangular in shape, which shows an electric double layer capacitor (EDLC) behavior. Figures 6(a)–(c) show the area under the curve of the NC 300 sample is higher than that of all the other samples. Similar observations are also made in respect of all the different scan rates. The specific capacitance of NC RT, NC 300, NC 400 and NC 500 was estimated from the CV curve using the equation [13]:

$$C_s = \frac{1}{mv(V_a - V_c)} \int_{-0.5}^{0.5} I\,(V)\ dV,$$

where C_s is specific capacitance (F g^{-1}), m is the mass of active material, υ is the scan rate (mV s^{-1}), V_a is the anode potential, V_c is the cathode potential, I is the current, V is the potential and integral area under the CV curves. The calculated specific capacitances for all the supercapacitors are plotted in figure 6(d). The specific capacitance decreased from 20 to 6 F g^{-1}, 324 to 57 F g^{-1}, 132 to 61 F g^{-1} and 81 to 48 F g^{-1} of the samples NC RT, NC 300, NC 400 and NC 500, respectively, with the increase in scan rate from 10 to 500 mV s^{-1}. The low capacitance at higher scan rate is because at lower scan rate electrolyte ions get enough time to accumulate on the electrode material, while at higher scan rate due to the faster polarity change, they did not have sufficient time for accumulation. The symmetric supercapacitor with NC 300 has a higher specific capacitance than the other samples.

The reduction of capacitance ($C = \epsilon_o \epsilon_r \left(\frac{A}{d}\right)$) with increasing pore size may be due to either a decrease in ε_r or an increase in d value. As pore size increases, pore flooding causes the 'solvation' as a result of the attraction between anions and cations being greater than that of the attraction

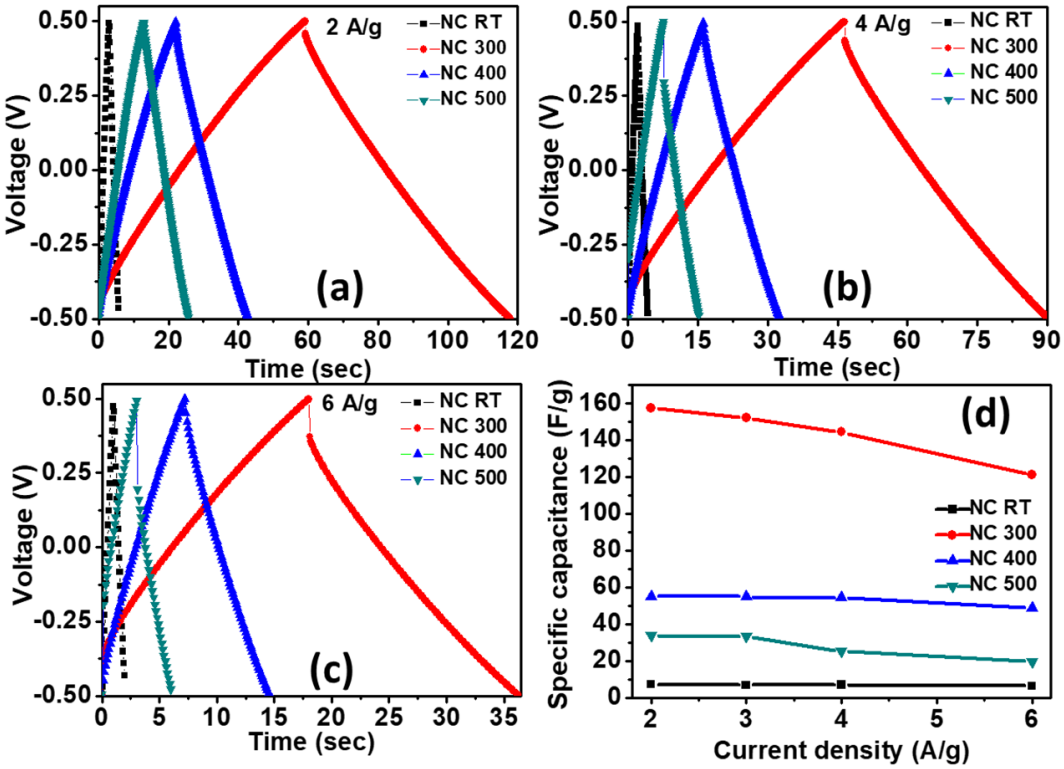

Figure 8. Charge–discharge plots of NC RT, NC 300, NC 400 and NC 500 at various current densities (a) 2 A g^{-1}, (b) 4 A g^{-1}, (c) 6 A g^{-1} and (d) specific capacitance versus current density.

between anions and the pore wall. As the attraction between anions and cations is greater than that of the attraction between anions and the pore wall, this causes the enhancement of d value in the samples, which causes the decrease in specific capacitance [23]. In the present case, NC 300 has 1.9 and 2.82 nm pores and NC 400 has 2.81 and 8.87 nm pores, while NC 500 has 2.12, 3.83 and 8.7 nm pores. Hence, it is found that the C_s of NC 300 is larger than that of NC 400 and NC 500. In addition, the decrease in specific capacitance of NC 400 and NC 500 is due to the decrease in surface area that occurs with increasing pore size. As pore size increases, the effective surface available is reduced causing decrement in capacitance. This can be seen in the large specific surface area of NC 300 (247.06 m^2 g^{-1}) compared to NC 400 (87.15 m^2 g^{-1}) and NC 500 (67.69 m^2 g^{-1}).

CV plots of the NC RT, NC 300, NC 400 and NC 500 samples that are further heated at 40 °C, 60 °C and 80 °C, after being cooled to 25 °C, are shown in figures 7(a)–(d). Figure 7(a) shows the perfect rectangular shape of the CV curve. In a similar way, the former samples show almost the same scan rate at these temperatures, which indicates the good stability of the supercapacitors at high temperatures. A symmetric supercapacitor comprising NC 300 displays better EDLC behavior at different working temperature than any other sample.

Figure 7(e) shows variation in specific capacitance with various temperatures of the symmetric supercapacitors. The C_s of the supercapacitors comprising NC RT and NC 400 is increased with the increase in temperature of the supercapacitor, while upon cooling to 25 °C decrement in C_s is observed. In the case of the NC 300 supercapacitor, C_s increases as its temperature increases by 4% (259 F g^{-1} at 60 °C), then again reduces at 80 °C. The C_s of the supercapacitor after cooling it to 25 °C is reduced by 31% (171 F g^{-1} at 25 °C). The NC 500 supercapacitor exhibits the same trend in supercapacitive behavior as the NC 300. The typical plot for cycling stability of the NC RT and NC 300 samples is shown in figure 7(f). The specific capacitance retention of the NC RT sample is 95.15%, while NC 300 shows 99.64% over 5000 charge–discharge cycles. This shows the excellent cycle stability of the NC composite calcined at 300 °C.

The galvanostatic charge–discharge plots of the NC RT, NC 300, NC 400 and NC 500 samples at various current densities viz. 2, 3, 4 and 6 A g^{-1} are presented in figures 8(a)–(c). The charge–discharge time of the supercapacitor decreases with an increase in calcination temperature of the NC composite, while NC RT has the lowest charge–discharge time. From the charge–discharge curve, NC 300 and NC 500 exhibit an IR drop, which may be due to the instant release of charge from the electrolyte/electrode interface. It can be seen that with an increase in current density, the IR drop increases. Figure 8(d) demonstrates the variation of specific capacitance with current density. Specific capacitance is calculated from the following equation [13]:

$$C_s = \frac{I\Delta t}{m\Delta V},$$

where, $\frac{I}{m}$ is the constant current density for discharge, Δt is the time of discharge and ΔV is the potential difference for discharge. The C_s values for NC RT, NC 300, NC 400

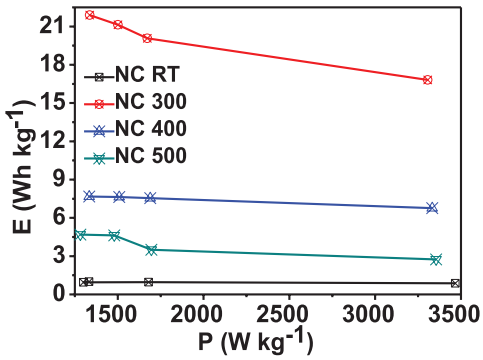

Figure 9. Ragone plots of energy density versus power density for NC RT, NC 300, NC 400 and NC 500.

and NC 500 are 7.17, 157 55.3 and 33.8 F g^{-1} at 2 A g^{-1}, which decreases to 6.3, 121, 48.6 and 19.7 F g^{-1} at 6 A g^{-1}, respectively.

Ragone plots are determined to compare the performances of surface currents depicting the relation between power density (W kg^{-1}) with its corresponding energy density (Wh kg^{-1}). The equations used for the calculation of energy density and power density are:

$$E = \frac{\frac{1}{2}C_s\Delta V^2}{3.6},$$

$$P = \frac{E}{t_d} \times 3600,$$

where C_s is the specific capacitance in F g^{-1} and ΔV is the potential difference for discharge. E is the energy density in Wh kg^{-1}, P is the power density in W kg^{-1} and t_d is the discharge time in seconds [17]. For measuring power density (P) and energy density (E), the IR drop is excluded from the potential value. The factors 3.6 and 3600 come from the unit conversions of time and mass from gram to kilogram and second to hour, respectively. Figure 9 shows the respective Ragone plots for NC RT, NC 300, NC 400 and NC 500. NC RT has the highest energy density 0.87 (Wh kg^{-1}) at a power density of 3467 (W kg^{-1}), while NC 300 possesses the highest energy density of 16.81 (Wh kg^{-1}) at a power density of 3306 (W kg^{-1}). This is due to fast voltage decay at higher power values.

Conclusion

A nanosheet of nickel and cobalt double hydroxides has been synthesized by the facile hydrothermal method. The LDHs are thermally treated to produce NiO–Co_3O_4 nanosheets. The appearance of the porous structure is due to the rapid release of water molecules during the transformation of both LDH to NiO and Co_3O_4 at elevated temperatures. A symmetric supercapacitor has been fabricated using NC composite. Among the supercapacitors, the symmetric supercapacitor comprising NC 300 has a higher capacitance of 324 F g^{-1} at a 10 mV s^{-1} scan rate. In addition, it shows excellent retention of 99.15% over 5000 cycles. The feasibility of synthesized material for a symmetric supercapacitor operating at a different temperature is evaluated. A symmetric supercapacitor comprising NC 300 displays good EDLC behavior at a different working temperature.

Acknowledgment

The authors acknowledge BRNS (Research project Number 34/14/05/2015/BRNS), Government of India for the financial support.

ORCID iDs

S K Mahapatra https://orcid.org/0000-0001-7370-3995

References

[1] Yan J, Fan Z, Wei T, Cheng J, Shao B, Wang K and Zhang M 2009 Carbon nanotube/MnO_2 composites synthesized by microwave-assisted method for supercapacitors with high power and energy densities *J. Power Sources* **194** 1202–7
[2] Arya A and Sharma A 2017 Insights into the use of polyethylene oxide in energy storage/conversion devices: a critical review *J. Phys. D: Appl. Phys.* **50** 443002
[3] Arya A and Sharma A 2017 Polymer electrolytes for lithium ion batteries: a critical study *Ionics* **23** 497–540
[4] Xia X, Tu J, Mai Y, Chen R, Wang X, Gu C and Zhao X 2011 Graphene sheet/porous NiO hybrid film for supercapacitor applications *Chem. Eur. J.* **17** 10898–905
[5] Wang X, Zheng D, Yang P, Wang X, Zhu Q, Ma P and Sun L 2017 Preparation and electrochemical properties of NiO–Co_3O_4 composite as electrode materials for supercapacitors *Chem. Phys. Lett.* **667** 260–6
[6] Wang H, Yi H, Chen X and Wang X 2013 Facile synthesis of a nano-structured nickel oxide electrode with outstanding pseudocapacitive properties *Electrochim. Acta* **105** 353–61
[7] Xia X-H, Tu J-P, Mai Y-J, Wang X-L, Gu C-D and Zhao X-B 2011 Self-supported hydrothermal synthesized hollow Co_3O_4 nanowire arrays with high supercapacitor capacitance *J. Mater. Chem.* **21** 9319–25
[8] Zhang Y, Xia X, Kang J and Tu J 2012 Hydrothermal synthesized porous $Co(OH)_2$ nanoflake film for supercapacitor application *Chin. Sci. Bull.* **57** 4215–9
[9] Zhang Y, Xia X, Tu J, Mai Y, Shi S, Wang X and Gu C 2012 Self-assembled synthesis of hierarchically porous NiO film and its application for electrochemical capacitors *J. Power Sources* **199** 413–7
[10] Lu X, Zhai T, Zhang X, Shen Y, Yuan L, Hu B and Zhou J 2012 WO_{3-x}@Au@MnO_2 core–shell nanowires on carbon fabric for high-performance flexible supercapacitors *Adv. Mater.* **24** 938–44
[11] Zheng H, Zhai T, Yu M, Xie S, Liang C, Zhao W and Lu X 2013 TiO_2@C core–shell nanowires for high-performance and flexible solid-state supercapacitors *J. Mater. Chem.* C **1** 225–9
[12] Chen H, Hu L, Chen M, Yan Y and Wu L 2014 Nickel–cobalt layered double hydroxide nanosheets for high-performance supercapacitor electrode materials *Adv. Funct. Mater.* **24** 934–42
[13] Liu P, Hu Z, Liu Y, Yao M, Zhang Q and Xu Z 2014 Novel three-dimensional hierarchical flower-like NiO–Co_3O_4 composites as high-performance electrode materials for supercapacitors *Int. J. Electrochem. Sci.* **9** 7986–96
[14] Liu T, Li Y, Quan G, Dai P, Yu X, Wu M and Li G 2015 Magnetic-field-assisted preparation of one-dimensional

(1D) wire-like NiO/Co_3O_4 composite for improved specific capacitance and cycle ability *Mater. Lett.* **139** 208–11
[15] Xu K, Zou R, Li W, Xue Y, Song G, Liu Q and Hu J 2013 Self-assembling hybrid NiO/Co_3O_4 ultrathin and mesoporous nanosheets into flower-like architectures for pseudocapacitance *J. Mater. Chem.* A **1** 9107–13
[16] Fan M, Ren B, Yu L, Song D, Liu Q, Liu J and Liu L 2015 Facile synthesis of Co_3O_4 nanowires grown on hollow NiO microspheres with superior electrochemical performance *Electrochim. Acta* **166** 168–73
[17] Zhou J-J, Wu M-K, Tao K, Li Y-L, Li Q, Chen C and Han L 2018 Tanghulu-like NiO microcubes on Co_3O_4 nanowires arrays anchored on Ni foam with improved electrochemical performances for supercapacitors *J. Alloys Compd.* **748** 496–503
[18] Jiang P, Wang Q, Dai J, Li W and Wei Z 2017 Fabrication of NiO@Co_3O_4 core/shell nanofibres for high-performance supercapacitors *Mater. Lett.* **188** 69–72
[19] Liu Z, Ma R, Osada M, Takada K and Sasaki T 2005 Selective and controlled synthesis of α-and β-cobalt hydroxides in highly developed hexagonal platelets *J. Am. Chem. Soc.* **127** 13869–74
[20] Yang J, Liu H, Martens W N and Frost R L 2009 Synthesis and characterization of cobalt hydroxide, cobalt oxyhydroxide, and cobalt oxide nanodiscs *J. Phys. Chem.* C **114** 111–9
[21] Windisch C F Jr, Exarhos G J and Owings R R 2004 Vibrational spectroscopic study of the site occupancy distribution of cations in nickel cobalt oxides *J. Appl. Phys.* **95** 5435–42
[22] Li J, Zhao W, Huang F, Manivannan A and Wu N 2011 Single-crystalline $Ni(OH)_2$ and NiO nanoplatelet arrays as supercapacitor electrodes *Nanoscale* **3** 5103–9
[23] Sillars F B, Fletcher S I, Mirzaeian M and Hall P J 2011 Effect of activated carbon xerogel pore size on the capacitance performance of ionic liquid electrolytes *Energy Environ. Sci.* **4** 695–706